University of Louisville
ThinkIR: The University of Louisville's Institutional Repository

Electronic Theses and Dissertations

7-2009

Synthesis of Molybdenum oxide nanowires and their facile conversion to Molybdenum sulfide.

Dustin Ray Cummins 1987-
University of Louisville

Follow this and additional works at: https://ir.library.louisville.edu/etd

Recommended Citation

Cummins, Dustin Ray 1987-, "Synthesis of Molybdenum oxide nanowires and their facile conversion to Molybdenum sulfide." (2009). *Electronic Theses and Dissertations.* Paper 300.
https://doi.org/10.18297/etd/300

This Master's Thesis is brought to you for free and open access by ThinkIR: The University of Louisville's Institutional Repository. It has been accepted for inclusion in Electronic Theses and Dissertations by an authorized administrator of ThinkIR: The University of Louisville's Institutional Repository. This title appears here courtesy of the author, who has retained all other copyrights. For more information, please contact thinkir@louisville.edu.

SYNTHESIS OF MOLYBDENUM OXIDE NANOWIRES AND THEIR FACILE CONVERSION TO MOLYBDENUM SULFIDE

By

Dustin Ray Cummins
B.S., University of Louisville, 2008

A Thesis
Submitted to the Faculty of the
J. B. Speed School of Engineering
in Partial Fulfillment of the Requirements
for the Professional Degree

MASTER OF ENGINEERING

Department of Chemical Engineering

July 2009

SYNTHESIS OF MOLYBDENUM OXIDE NANOWIRES AND THEIR FACILE CONVERSION TO MOLYBDENUM SULFIDE

Submitted by: _____

Dustin Ray Cummins

A Thesis Approved on

_____

(Date)

By the Following Reading and Examination Committee

_____

Dr. Mahendra K. Sunkara (Thesis Director)

_____

Dr. Gerold Willing

_____

Dr. Gamini Sumanasekera

ACKNOWLEDGEMENTS

I am foremost indebted to my mother. Without her constant love and support, my education would not have been possible. I would also like to extend a great thanks to Dr. Mahendra Sunkara. His guidance, assistance, and support have been invaluable to me. He has shown personal involvement with my well being, both in my educational endeavors and my life outside the classroom.

Other member of the faculty at the University of Louisville have helped me along the way with their advice and support, particularly, Dr. Gerold Willing, Dr. Jim Watters, Dr. Gamini Sumanasekera, Dr. Walden Laukhuf, and many others.

I would like to thank everyone in my lab group who helped me with my work, with either advice or merely their friendship. Thanks to Suresh Gubbala, Chandrashekhar Pendyala, Praveen Meduri, Rupa Dumpala, Ben Russell, Vivek Kumar, Jyotish Thangala, Jeong Kim and Boris Chernomordik. I'd also like to thank Rodica McCoy, Dr. Biswa Deb and Dr. Jacek Jasinski for their assistance.

Finally I would like to acknowledge my brothers in Triangle Fraternity. Without them, I would not have been able to survive the stresses of my engineering education. They have taught me to work hard and accomplish great things, but to have fun will I do it.

ABSTRACT

The future of renewable energy technologies involves overcoming difficulties with the creation of new materials. The use of nanotechnology has allowed for inexpensive materials to achieve very interesting physical and electronic properties. This thesis investigates the synthesis Molybdenum oxide nanowire arrays are synthesized using HFCVD, then converted to Molybdenum sulfide under relatively benign conditions. These inexpensive nanowires have applications in photovoltaics, Li ion batteries and much more.

Molybdenum oxide nanowire arrays were successfully synthesized. The nanowires had an average length of 0.5 microns and an average diameter ranging from 10 to 20 nm. The primary focus of this thesis was the post synthesis of these oxide nanowires to Molybdenum sulfide. The MoO_3 nanowires were reacted with pure H_2S at relatively low temperatures, ranging 200 – 300°C. This conditions successfully synthesized MoS_2 nanowires. Reaction conditions at these low temperatures differ greatly from the normal method of MoS_2 synthesis which require extreme conditions and do not produce a nanowire morphology. These sulfide nanowire arrays have applications in photovoltaics due to its low band gap of 1.7 eV and also as a cathode material for Li ion batteries.

TABLE OF CONTENTS

LIST OF FIGURES

I. INTRODUCTION

The development of energy efficient renewable energy technologies critically depend on our ability to understand and develop new materials. Materials, especially semiconductors, have significantly improved electrochemical and physical properties when given nano-scale morphologies, when compared to bulk characteristics. Such materials will need to come from earth abundant compounds for widespread application for global energy demands. In this thesis, one-dimensional forms of Molybdenum oxide is deposited on substrates. The MoO_3 nanowire arrays are then reacted at low temperatures (200-300°C) with hydrogen disulfide to form Molybdenum sulfide nanowire arrays. These MoS_2 arrays have interesting properties and will be useful in many applications.

Molybdenum oxide is a relatively inexpensive semiconductor material. MoO_3 is a n-type semiconductor and has many applications. It can be used as a catalyst, gas sensing applications, solid lubricants, and electrochromic applications. Recently, advances have been made in using MoO_3 as an anode in Li-Ion battery technology. Li-Ion batteries operate by using lithium ions to charge a metal oxide framework, then discharge electrons to produce energy. The basic chemical reaction that takes place in the battery is

$$MO + Li^+ + e^- \leftrightarrow Li_2O + M$$

Where MO is the metal oxide and M is the discharged metal. A group at the National Renewable Energy Laboratory (NREL) has shown that MoO_3 can accommodate up to 6 Li ions and the reduced form, MoO_2, can support 4 ions. As a comparison, commercial Li-ion batteries use a graphite anode which can only accommodate 1 Li ion. MoO_3 anodes have been shown to have a capacity of 1117 mAh g^{-1}, compared to commercial

graphite anodes with a capacity of only 372 mAh g^{-1}. The use of MoO_3 anode materials shows significant improvement in both current and potential over commercial graphite. These improvements were seen using MoO_3 that were ball-milled to the micron scale. [1] If these anode materials can be synthesized with nano-scale morphologies, their applications in battery technology should very interesting.

Molybdenum sulfide has also been shown to be a promising material for Li-Ion battery technology, in this case as a cathode material. It has been shown that MoS_2 has a very high mobility for Lithium ions and high charge storage capacity. Also, MoS_2 is a resilient material in that decrease in voltage in the battery after over 100 cycles very minimally. [2]

Molybdenum sulfide nano-structures have been shown to be applicable in hydrogen storage applications. These nano-morphologies can reversibly store hydrogen by both gaseous and electrochemical techniques. The excellent cathode properties of MoS_2 allows for the electrochemical storage of hydrogen at 0.97 wt%. [3] Also, nanostructure of molybdenum sulfide have shown 1.2 wt% gaseous storage of hydrogen. [4]. Molybdenum and its compounds are earth abundant materials and are relatively inexpensive; these materials are great candidates for renewable energy applications, in both generation and storage.

This thesis involves the synthesis of Molybdenum oxide nanowire arrays by HFCVD. These arrays are then reacted with hydrogen disulfide to produce Molybdenum sulfide nanowires. The reaction is carried out at lower temperatures and the resulting nano-arrays can be used for electrochemical applications.

The remaining chapters of this thesis are as follows:

The second chapter provides an extensive background on nanowire synthesis mechanisms. Then, past work on the sulfurization of molybdenum oxide to sulfide is discussed.

The third chapter discusses the reactors used in the synthesis. A Hot Filament CVD reactor was used to produce the oxide nanowire arrays, then a smaller reactor was used to react the nanowires with hydrogen disulfide to produce the molybdenum sulfide nanowires. Also, the instruments used for characterization are discussed along with the general theory behind their operation.

The results are discussed in the fourth chapter. This includes the determination of proper reactor conditions, for both the oxide and sulfide synthesis, and also the results of the characterization techniques. The remaining chapters present the conclusions of this thesis and recommendations for further improvement of the work.

II. THEORY AND BACKGROUND

Work on one dimensional nano-scale growth was begun in the 1940's and research still continues today. The two predominant mechanisms for nanowire growth are the well explored, Vapor-Liquid-Solid (VLS) approaches, and Vapor-Solid (VS) mechanism. The synthesis of the molybdenum oxide nanowires appear to follow the Vapor-Solid mechanism.

A. Vapor-Liquid-Solid Mechanism

Wagner and Ellis first proposed the Vapor-Liquid-Solid mechanism for one dimensional crystal growth. In their experiments, gold droplets were deposited onto a silicon substrate. The system was heated to a high temperature in a silane gas environment. The silane vapors would diffuse into the molten gold droplets. The silane would decompose in the gold droplets, which would become supersaturated with silicon. Because of the supersaturation, the silicon will nucleate and deposit as a crystal. The gold droplet acts as a catalyst and guide for the nucleation and crystal growth in one dimension. A diagram of the growth mechanism can be seen in

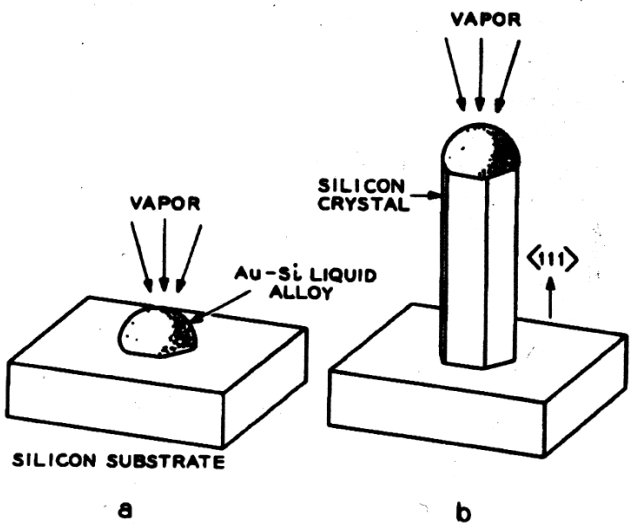

Figure 1. Schematic of growth of a Silicon crystal by VLS. a) The initial stage in which the liquid droplet is being saturated. b) Growth of the crystal with the droplet on top. [5]

Figure 1. During the initial stage (Figure 1a), the molten gold droplet is becoming saturated with the silicon vapor. Once the supersaturation point is reached, crystal growth begins (Figure 1b). The diameter of the one dimensional nanostructure, referred to as a "whisker" or "nanowire" is dictated by the diameter of the molten gold catalyst droplet. Trace amounts of the molten catalyst droplet is deposited with the nanowires, so the crystal can grow until the liquid droplet is used up, but the growth is usually stopped well before that point by removing the vapor phase. [5]

The growth of these nano-whiskers is dominated by the thermodynamic instability due to the supersaturation of the molten gold droplet. The thermodynamic instability involved with the supersaturation is described by the chemical potentials (μ). The chemical potential quantitatively describes the thermodynamic equilibrium conditions between phases for each material. Chemical potential is a function of the temperature, pressure, and the composition of the system. Chemical potential of any system cannot be measured directly, but must be calculated relative to some reference potential at a standard temperature and pressure. The ideal chemical potential for a component is described by

$$d\mu_i = -s_i dT + \mathbf{v_i dP} \qquad (1)$$

in which μ_i is the chemical potential of a particular component, s_i is the molar entropy, and v_i is the molar volume of each species. To explain nonideality in the thermodynamic system, whether a pure species or a mixture, the isothermal change in chemical potential can be described by the fugacity (f).

$$\mu_i - \mu_i^0 = RT \ln \frac{f_i}{f_i^0} \quad (2)$$

In this equation, μ_i^0 or f_i^0 are arbitrarily chosen at some standard state; they are not independent because by choosing the standard state for one parameter, the other is set. [6]

Knowledge of the chemical potential of the system can be used to describe the thermodynamic conditions that lead to nanocrystalline growth. The Gibbs Thompson relationship describes the chemical potential gradient at the surface of the molten catalyst droplet:

$$\Delta\mu = \Delta\mu^0 - \frac{4\Omega\alpha}{d} \quad (3)$$

In this equation, $\Delta\mu$ is the change in the chemical potential at the curved surface of the droplet, $\Delta\mu^0$ is the change in the chemical potential on a flat plane, Ω is the molar volume, α is the interfacial energy, and d is the diameter of the growing nano-whisker. This calculated chemical potential, which quantitatively describes the changes in equilibrium and the state of supersaturation, can be used to estimate nanowire growth rate, "V", from an empirical relation.

$$V = b\left(\frac{\Delta\mu}{kT}\right)^n \quad (4)$$

In which, "b" is a constant independent of supersaturation, "n" is obtained from experimental data, and "k" is the Boltzmann Constant. This model for growth by the VLS mechanism was proposed in 1975 by Russian researched Givergizov. In this model, he only describes the vapor solid interactions and neglects the vapor liquid interactions, for the sake of simplification. This model differs from experimental results because of this simplification. [7]

Expanding upon Givergizov's model, the VLS mechanism can be derived using thermodynamic models for solutions. The Gibb's Energy of mixing is calculated for the species involved to determine the deviation from equilibrium. The chemical potential of any species in the system is equal to the partial molar Gibb's energy of that component.

$$\bar{G}_i = \mu_i = \mu_i^0 + RT \ln \gamma_i X_i \qquad (5)$$

where γ_i is the activity coefficient for the component and X_i is the molar fraction of the component. The activity describes the changes in enthalpy and entropy due to non-ideal interaction with component "i" with the other species in the system. After some simplification, the Gibb's Energy of mixing for a two component system is described by

$$\Delta G = RT(X_A \ln \gamma_A X_A + (1 - X_A) \ln \gamma_B (1 - X_A)) \qquad (6)$$

If the assumption is made that the solution is ideal, i.e. that any interactions between the solute and solvent do not differ from the interactions in a pure state, then the interactive activity of each component is proportional to its mole fraction. The assumption of

ideality cause the activity coefficient, "γ", of each component to be equal to 1. Thus, the Gibb's energy of mixing for this ideal solution is

$$\Delta G = RT(X_A \ln X_A + X_B \ln X_B) \quad (7)$$

The Gibb's free energy of mixing can be used to give a better estimate of the chemical potential of the system and the interactions between the solute and solvent. [7]

B. Vapor-Solid Mechanism

While the growth of many one dimensional nanostructures can be attributed to the VLS mechanism, many other materials do not form by this method. Upon examination, there is no presence of the molten catalyst metal droplet. These nanowires, particularly metal oxides, deposit directly from the vapor phase to the solid phase. This mechanism is described as Vapor-Solid mechanism.

This mechanism was first described by Frank in 1949. Frank describes the Vapor-Solid (VS) mechanism and the one dimensional crystal growth as a result of dislocations and defects in the crystal. Similar to VLS, the supersaturation of the vapor species leads to a thermodynamic driving force; the dislocation in the crystal structure acts as a nucleation site. Dislocations in a crystal lattice can be many shapes and directions, and the direction and morphology of the resulting crystal growth depends directly on the type of defect. A typical annealed metal crystal has an average of 10^8 dislocation lines intersecting per square centimeter. A sample with this many dislocations may be seen as high perfection using x-ray diffraction, but the impurities and imperfections inherent in metals will lead to dislocations. Depending on the direction and angle of the dislocation line intersections, many different dislocations can be seen. When a dislocation is curved, it is known as a "screw dislocation". If the screw dislocation occurs toward the center of the crystal face, then, under supersaturated conditions, the dislocation can continue to spiral upwards, like a staircase. This forms relatively one dimensional structures. A block diagram of a screw dislocation can be seen in Figure 2. Theoretically, as long as the supersaturated conditions exist, the crystal growth can be indefinite. Because of the

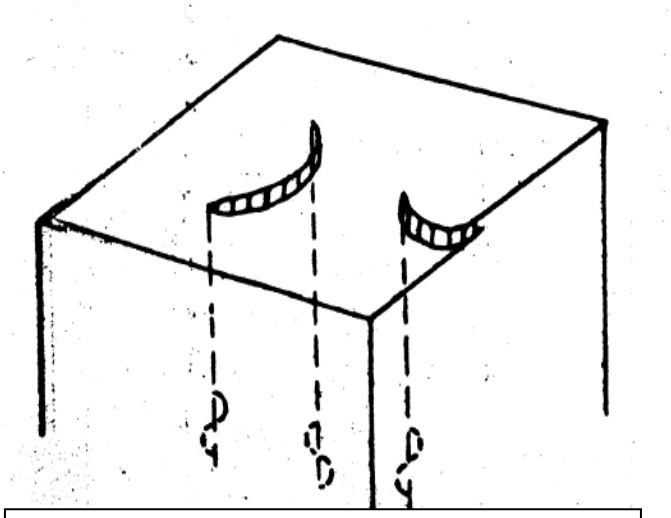

Figure 2. Screw dislocations in a crystal face. [8]

screw dislocation guiding the growth, the spiral crystal has a critical radius which it cannot exceed. The critical radius is dependent on the binding energy of the crystal and the extent of supersaturation of the system. The best growth conditions occur under low supersaturation concentrations. [8]

Frank's proposed mechanism assumes that dislocations and defects are present in the crystal, which propagates the growth. This self-propagating mechanism is seen in many metallic compounds, such as cuprite and aluminum nitride. However, there are many experimental instances of single crystal nanowires, in which no screw dislocations are found. Also, it has been found that only micron scale crystals can be produced by this dislocation mechanism, due to the dislocation dominating the growth direction and size. [9] However, a modified VS mechanism can be used to describe one dimensional crystal growth. This mechanism also relies on the thermodynamic driving force due to the supersaturation in the vapor phase. Under high temperature conditions, the solid sublimes, decomposes, and condenses. The nanowire morphology comes from the balance of the rates of these processes. Supersaturation, "S" is described as the ratio of the partial pressure of the solid in the vapor phase, "p", over the equilibrium vapor pressure of the solid, "p_e".

$$S = \frac{p}{p_e} \qquad (8)$$

The driving force due to this supersaturation is described by the chemical potential gradient.

$$\Delta\mu = kT \ln S \qquad (9)$$

At equilibrium, there is no growth and the chemical potential gradient is zero. During condensation, the partial pressure of the solid in the vapor phase is greater than the vapor pressure at equilibrium, so the chemical potential gradient is positive. During sublimation, the equilibrium vapor pressure is greater than the sublimed solid pressure, so the chemical potential gradient will be negative. Compared to the VS mechanism involving the screw dislocation, which requires low supersaturation, the growth by VS mechanism without the dislocation requires significantly high supersaturation levels. [10] This mechanism based on supersaturation can only account for growth rates observed but cannot account for the observed one-dimensional morphology.

The one dimensional morphology can be described by the temperature of the deposition and the relative rates of condensation and decomposition. When the temperature is very high, the rate of decomposition is higher than the rate of vapor condensation, so the crystal structure will be tapered, like a needle. Under moderate temperatures in which the rate of condensation and decomposition are similar, then the one dimensional crystal will have a more uniform diameter, leading to nanowires. At lower temperatures, the rate of condensation of the vapor is significantly higher than the rate of decomposition, so nanocrystals and nanoparticles are formed, rather than the one dimensional morphology. [11]

3. Molybdenum sulfide synthesis

There are also a variety of methods for the synthesis of semiconductor sulfide nanostructures, particularly Molybdenum sulfide. Molybdenum sulfide nanowires are most commonly synthesized as a precipitate from a precursor solution. Also, Molybdenum sulfide is also synthesized chemically with molybdenum or molybdenum oxide as a template.

Nagaraju et al. reacted a molybdenum precursor, ammonium molybdate, with a sulfur source in an acid solution at 180°C. The sulfur source used was either sodium sulfide crystals, or hydrogen sulfide was bubbled through the system briefly. This reaction lasted between 24 and 48 hours and yielded nanofiber bundles. In order to extract the nano-bundles, the resulting solution was centrifuged to separate the black precipitate, which was then washed with water and ethanol and dried. [12] Another group used an ammonium thiomolybdate [$(NH_4)_2MoS_4$] solution in conjunction with surfactants. The thiomolybdate was dissolved in water and the solution was reduced by bubbling hydrogen sulfide. Once reduced, surfactants were added to exceed the critical micelle concentration. Once the critical micelle concentration was reached, the templated sulfide precipitated out, and the precipitate was filtered out, washed and dried at high temperatures under a reducing atmosphere containing H_2S. This method of synthesis yields a tube like morphology, but also has sheets of polycrystalline MoS_2. Also, the presence of remaining surfactant template was detected as an impurity [13]. This method leads to inconsistent resulting morphologies and requires significant cleaning to obtain a pure sulfide product.

Templating is a common technique of nanowire synthesis. Yifeng Shi et al. utilize mesoporous silica templates to form sulfide nanostructures. Triblock copolymers,

a molybdic acid precursor and a sulfur source were all reacted in the presence of the mesoporous template at 600°C for 5 hours. This yields highly oriented nanostructures [14]. This method also requires high temperatures and removal of a template. Also, reactions become more complicated in using precursors. A diagram of the templating process can be seen in Figure 3. This figure shows the synthesis technique for tungsten sulfide nanowires, but molybdenum sulfide synthesis is carried out in the same way, with the use of molybdenum precursors.

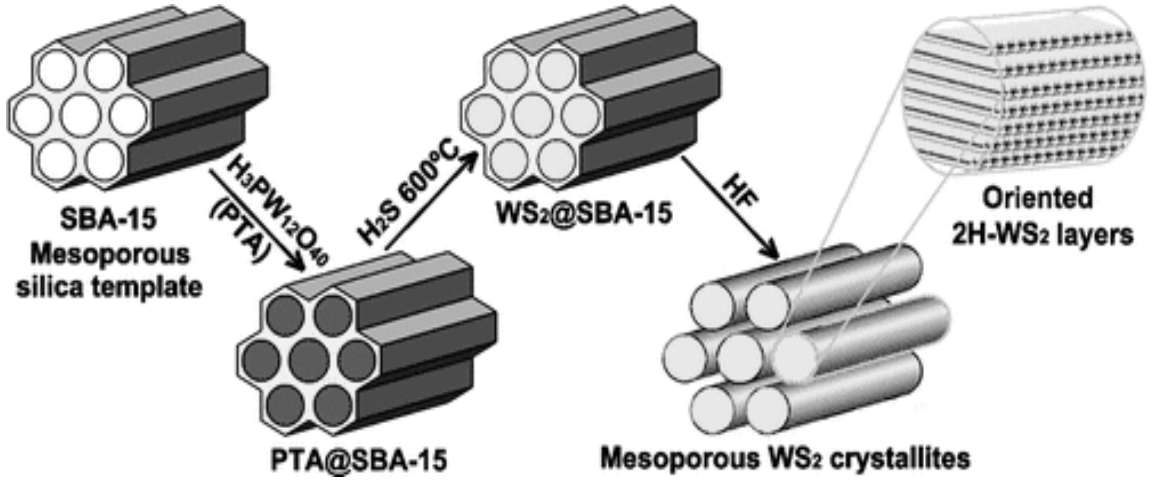

Figure 3: A diagram of sulfide nanowire synthesis using a templating technique. This shows the synthesis of WS_2 nanowires, but MoS_2 wires are formed by the same process. [37]

Some researchers have converted MoO_3 nanostructures directly to MoS_2. One group formed molybdenum oxide nanostructures using thermal decomposition of a molybdenum precursor, ammonium molybdate. Once the oxide nanostructures were formed, they were reacted in a reducing atmosphere of Argon and H_2S. This reaction took place at 800°C for 1 hour. This yielded MoS_2 fullerenes and nanotubes. [15] A disadvantage of this technique is the very high temperatures at which the reaction must be conducted. This research also put forth that the growth mechanism of the sulfurization reaction involves the formation of a sulfide around the oxide structure. Thus, nanowire

oxides will yield tubules of sulfide, while oxide nanospheres will create sulfide fullerenes during the reaction. [15] The approach of this thesis is to use simple and inexpensive processes to synthesize ordered nanowire arrays for use in many electrochemical applications.

III. EQUIPMENT AND EXPERIMENTAL PROCEDURES

This chapter discusses the reactor and procedure used to synthesize the molybdenum oxide nanowire arrays, and then the reactor and procedures for converting the molybdenum oxide to molybdenum sulfide. Once the materials have been synthesized, they must be characterized, so those instruments are also described in this chapter.

A. Hot Filament Chemical Vapor Deposition Reactor

In order to synthesize molybdenum oxide nanowire arrays in bulk, a hot filament chemical vapor deposition reactor was utilized. This reactor was earlier used for bulk synthesis of tungsten oxide nanowires. [16] A photo of the reactor can be seen in Figure 4.

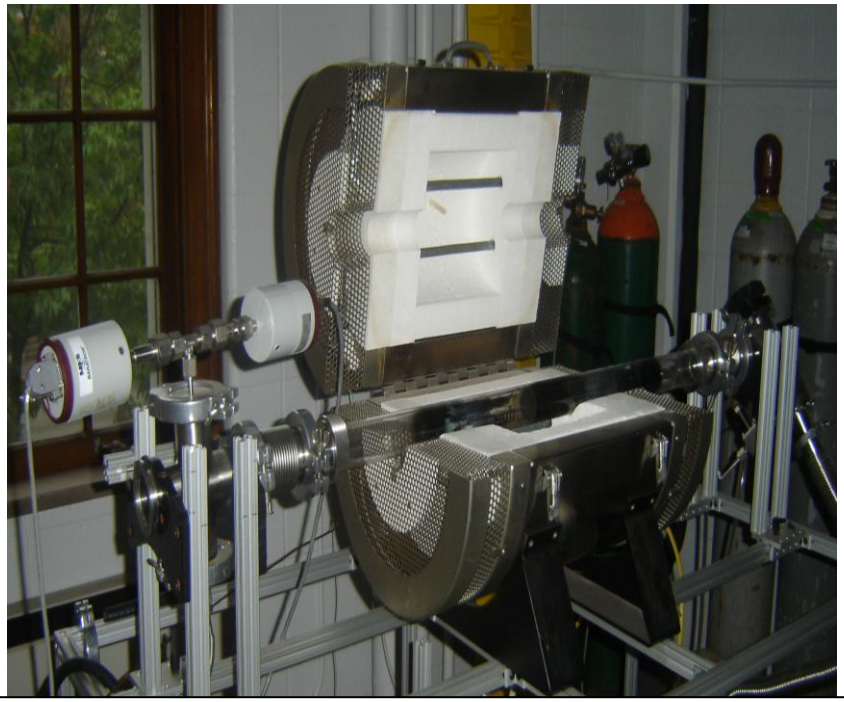

Figure 4: A photo of the HFCVD reactor. The reaction occurs in the 2" quartz tube. The large metal furnace surrounding the tube was not used during this experiment.

The hot filament reactor utilizes two spools of molybdenum wire coiled around boron nitride tubes. An image of the filament coiled around the boron nitride tubes can be seen in Figure 5.

Figure 5: A photo of the Mo filament coiled around boron nitride tubes. The heating rods can be seen at the right hand side of the photo. The boron nitride tubes are blue due to MoO_3 deposition.

The boron nitride tubes are light blue because of the molybdenum oxide deposits from the reaction. These tubes are attached to molybdenum heating rods, which can be seen at the right edge of the Figure 5; they play no part in the reaction other than allowing connecting to the copper contacts to allow voltage to flow through the molybdenum coils. Molybdenum

Figure 6: Detail of the electrical connection of the filament to the heating rods via molybdenum nuts.

nuts acted as the contacts for the wire coils. Molybdenum was used for the heating rods because of its relatively high melting point. A detail of the electrical connection of the molybdenum wire coil to the heat rods via the nuts can be seen in Figure 6.

The substrates, which can be either FTO glass or quartz pieces, are placed into a 1.75" quartz tube, which is then placed inside the 2" quartz tube. Both the molybdenum wire coils and the substrates will be contained within this smaller tube, with approximately 0.5" between the molybdenum coils and the substrates. The reason for placing the reaction inside a smaller quartz tube is due to the sputtering of molybdenum oxide in all directions. A smaller quartz tube can be removed more easily for cleaning, rather than disassembling the entire reactor set-up. This ease of cleaning eliminates cross contamination between different experiments. A schematic can be seen in Figure 7.

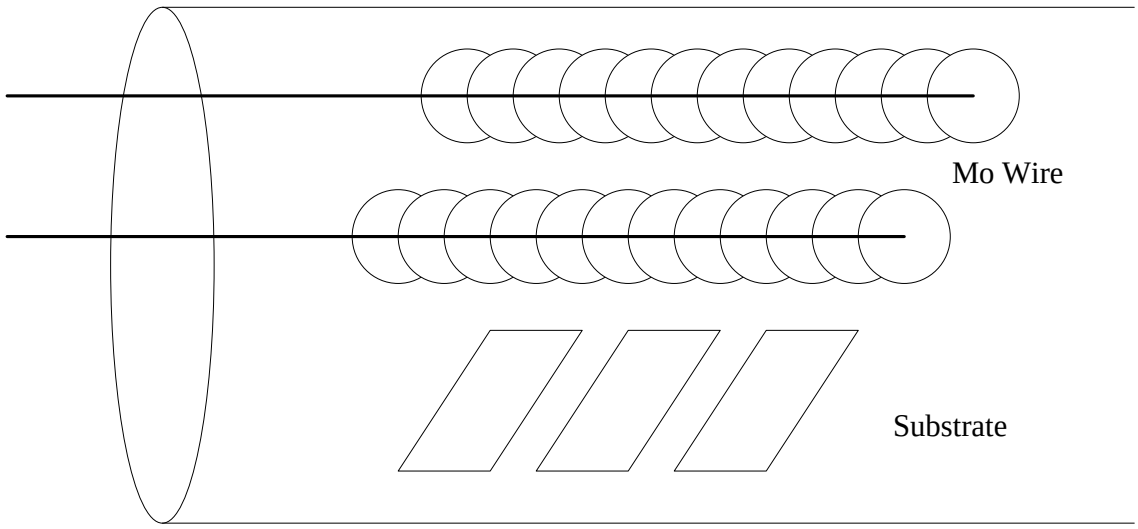

Figure 7: A schematic of the hot filament CVD reactor. The Mo wire is coiled around Boron Nitride tubes, and placed in contact with Mo rods.

Care must be taken that the molybdenum filament does not come into contact with the inner quartz tube, as the filament will quickly burn out. Since the reactor setup, including

the molybdenum heating rods, the boron nitride tubes, and the wire coils, is over three feet long, it tended to sag, causing the filament to touch the quartz tube. To prevent this, a 1 cm thick alumina disk was added as a support for the molybdenum heating rods.

A 20 sccm on a nitrogen basis MFC was used to pump oxygen into the reactor. The MFC was model 1160A from Unit Instruments and was connected with a card adapter to an MKS 247 four channel power supply and readout box.

The vacuum pump used for this system is a Maxima C Plus Vacuum Pump from Fisher Scientific, Model M8C. The pressure of the reactor was measured by two pressure gauges, MKS Baratron Model 627A; one with a range of 100 Torr, the other a range of 1 Torr. Each pressure gauge had a readout, MKS Type 250 Controller.

B. Nanowire Array Growth

The substrate used in this experiment was either quartz or FTO conducting glass. Regardless of substrate used, the pieces were approximately 2 cm by 2 cm. Typically 4 to 6 substrate pieces were placed in the 1.75" diameter quartz tube, which was then inserted into the larger 2" quartz tube. The electric apparatus, which includes the heating rods, boron nitride tubes and coiled filament, is inserted into the larger quartz tube and positioned within the smaller tube, approximately 0.5" from the substrates. Care must be taken that the filament is not in contact with the quartz tube when the voltage is applied.

The system is pumped down and purged with pure oxygen. Oxygen was flowed into the system at a rate of 10 sccm. Voltage was applied to the filament via a Variable Voltage Regulator, with a maximum capacity of 130 V. A potential between 20 and 25 volts were applied to the filament, yielding a current of 8 amps. The voltage applied was

not always the same for each experiment because as the filament was used, it would become thinner and develop hot spots and imperfections in the wire. This would cause a drop in current through the wire, even though the same voltage was applied. The goal was to keep the system at 200 Watts, which lead to a filament temperature of 775°C, which was measured by pyrometer. This temperature was found to be ideal for nanowire synthesis by trial and error. If the temperature was too high, a nano-particle morphology was observed. If the filament temperature was too low, then there would not be enough deposition to form any structure. Once the desired filament temperature was reached, the reaction ran for 30 minutes, at an operating pressure of 0.7 to 0.9 Torr. Once the reaction was complete, the voltage was slowly turned off and the reactor was allowed to cool under vacuum until the system is at room temperature.

Once cooled, the reactor is vented and the filament heating apparatus is removed. A large copper rod is inserted into the reactor and is used to slid the smaller quartz tube out. The substrates are removed and the quartz tube is soaked in a water bath for cleaning.

C. Sulfurization Reactor

Once the molybdenum oxide nanowire arrays have been deposited onto the substrate, the sample is placed into the sulfurization reactor to be converted to molybdenum sulfide nanowires. This reactor involves a boron nitride heating plate in a H_2S atmosphere. A photo of the reactor can be seen in Figure 8.

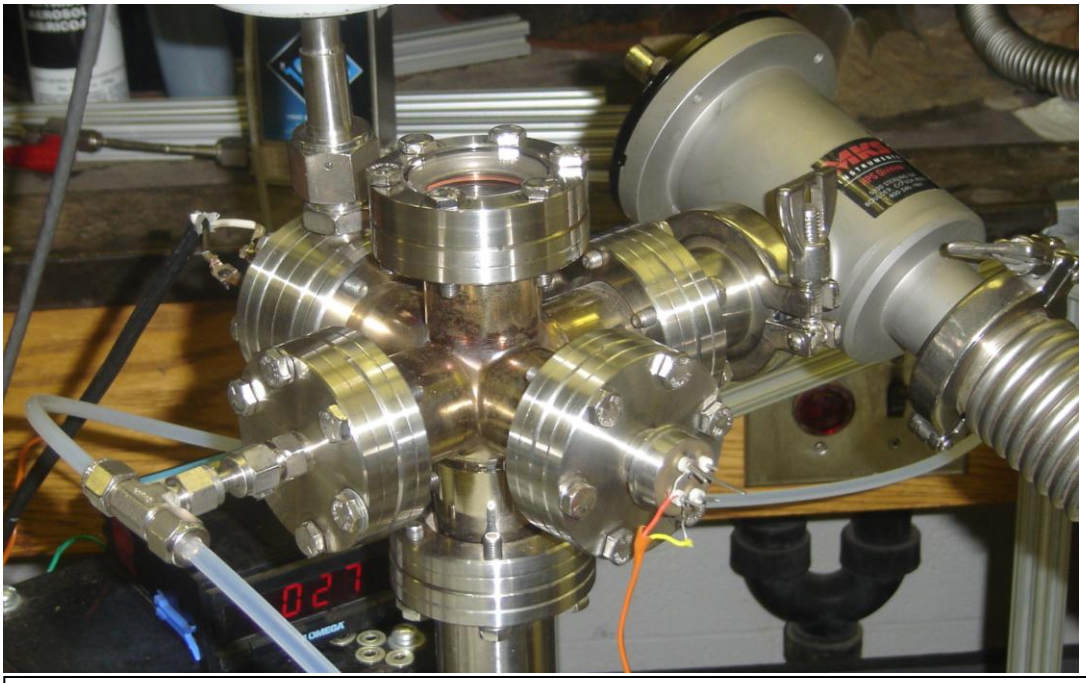

Figure 8: A photo of the sulfurization reactor

The reactive gas enters through the Teflon tubing on the left of the reactor. The sample is inserted through the flange at the top of the reactor and is lowered onto a boron nitride heating stage at the center of the reactor. The electrical connections for the heating stage can be seen coming into the rear of the reactor, while the electrical connections at the front are for the thermocouple, which positioned directly below the heating stage. A schematic of the layout of the heating stage within the reactor can be seen in Figure 9.

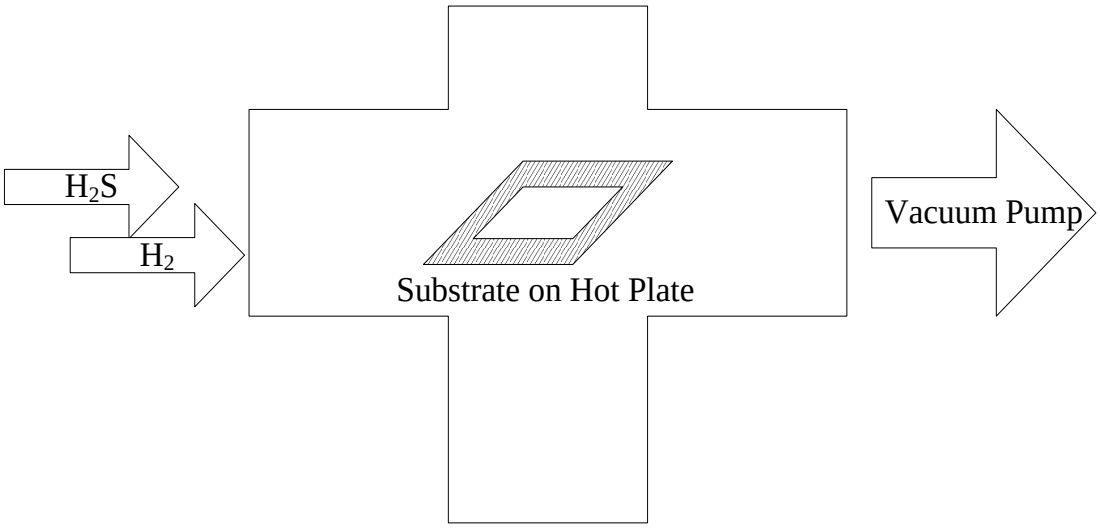

Figure 9: A schematic of the sulfurization reactor. The substrate is placed on a boron nitride hotplate and the reactive gases are passed over the substrate.

The reactor chamber is T-shaped stainless steel with 2.75" ConFlat Flanges. The reaction chamber has an approximate volume of 22.5 cm^3. The reactive gas is pumped into the chamber using a MFC. This MFC is a Type 1660 Metal ZSeal™ by Unit Instruments calibrated to deliver 25 sccm of pure H_2S. Pure Hydrogen disulfide gas is fed to the MFC from a 3 lb. net weight lecture bottle.

D. Material Characterization

The physical and electrochemical properties of the nanowire arrays were determined using scanning electron microscopy (SEM), X-Ray diffraction (XRD), UV-Visible spectroscopy, and also Raman Spectroscopy and Photoluminescence (PL).

1. Scanning Electron Microscopy

Scanning Electron microscopy (SEM) is a crucial tool in the characterization of the topography of a sample on the nanoscale. SEM works by bombarding the sample surface with electrons. When the electron interacts with the sample, it can be reflected,

which is known as a backscattered electron, or it can interact with the sample and cause the emission of a secondary electron, and Auger electron, or an X-ray. Each of these emissions can be collected by the proper detector to characterize the sample. In SEM, the secondary electrons are collected and used to produce a topographical image.

In a typical SEM, an electron beam is thermionically emitted from an electron gun fitted with a tungsten filament cathode. Tungsten is normally used in thermionic electron guns since it has the highest melting point and lowest vapor pressure of all metals and because of its low cost. Other types of electron emitters include lanthanum hexaboride cathodes, which can be used in a standard tungsten filament SEM if the vacuum system is upgraded and field emission guns. The electron beam, which typically has an energy ranging from a few hundred eV to 40 keV, is focused by one or two condenser lenses to a spot about 0.4 nm to 5 nm in diameter. The beam passes through pairs of scanning coils or pairs of deflector plates in the electron column, typically in the final lens, which deflect the beam in the *x* and *y* axes so that it scans in a raster fashion over a rectangular area of the sample surface. [17]

When the primary electron beam interacts with the sample, the electrons lose energy by repeated random scattering and absorption within a volume of the specimen known as the interaction volume, which extends from less than 100 nm to around 5 μm into the surface. The size of the interaction volume depends on the electron's energy, the atomic number of the specimen, and the specimen's density. The energy exchange between the electron beam and the sample results in the backscattering of high-energy electrons by elastic scattering, emission of secondary electrons by inelastic scattering, and the emission of electromagnetic radiation, each of which can be detected by

specialized detectors. The beam current absorbed by the specimen can also be detected and used to create images of the distribution of specimen current. Electronic amplifiers of various types are used to amplify the signals which are displayed as variations in brightness on a cathode ray tube. The raster scanning of the CRT display is synchronized with that of the beam on the specimen in the microscope and the resulting image is therefore a distribution map of the intensity of the signal being emitted from the scanned area of the specimen. [17]

Backscattered electrons (BSE) consist of high-energy electrons originating in the electron beam that are reflected or back-scattered out of the specimen interaction volume by elastic scattering interactions with specimen atoms. Since heavy elements backscatter electrons more strongly than light elements, and thus appear brighter in the image, BSE are used to detect contrast between areas with different chemical compositions. The Everhart-Thornley detector, which is normally positioned to one side of the specimen, is inefficient for the detection of backscattered electrons because few such electrons are emitted in the solid angle subtended by the detector, and because the positively biased detection grid has little ability to attract the higher energy BSE electrons. Dedicated backscattered electron detectors are positioned above the sample in a "doughnut" type arrangement, concentric with the electron beam, maximizing the solid angle of collection. BSE detectors are usually either of scintillator or semiconductor types. When all parts of the detector are used to collect electrons symmetrically about the beam, atomic number contrast is produced. However, strong topographic contrast is produced by collecting back-scattered electrons from one side above the specimen using an asymmetrical, directional BSE detector; the resulting contrast appears as illumination of the topography

from that side. [18] Since the samples imaged in these experiments were of uniform composition, backscattered imaging was not necessary.

For effective surface imaging, the sample should be electrically conductive. Metallic samples and conductive compounds, such as MoS_2, can be easily imaged by secondary electrons. But non-conductive samples and most undoped semiconductors, such as MoO_3, cause the sample to charge, that is that electrons accumulate on the surface of the sample, which inhibits imaging. To overcome the problem of charging, a nonconducting sample is usually coated in a thin layer of metal, usually gold by sputtering. Sputtering, however, permanently chemically contaminates the sample, so a technique of scrapping the nonconducting sample onto a gold sputtered substrate for imaging can also be used.

The SEM used for these experiments was the Nova 600 NanoSEM by FEI with a field emission gun. The secondary electron detector used was a TLD detector in immersion mode for high resolution images.

2. X-Ray Diffraction

X-Ray Diffraction (XRD) is a characterization technique to determine the crystal structure of a material. X-rays are produced by a tungsten filament, which is heated and bombards a target, usually copper to produce x-rays. The x-rays hit the sample and, if the sample is crystalline and has the proper atomic spacing, then constructive and destructive interference occurs. In order for the incident x-ray to be diffracted, the scattered ray must satisfy Bragg's Law, which is

$$n\lambda = 2d\sin\theta \qquad (10)$$

The wavelength of the monochromatic incident x-ray, λ, must strike penetrate the sample to a certain depth, d, and at a specific angle, θ, to be diffracted.[19] The XRD apparatus involves two movable arms that revolve around a stage. One arm is the x-ray emitter, while the other is a collector. The angle between the emitter and the detector is measured as 2θ. The intensity of the diffracted x-ray is plotted versus 2θ, and the spectrum can be used to determine chemical composition and crystal structure. The XRD used for these experiments is the Bruker AXS D-8 HR XRD

3. UV- Visible Spectroscopy

UV- Visible Spectroscopy (UV-Vis) is a technique to determine the band gap of a material by exposing the sample to light ranging from Ultraviolet to the near Infra-Red and measuring the adsorption of each wavelength.

Transitions of electrons between outermost energy levels are associated with energy changes in the range of 10^4 to 10^5 cm^{-1} or 10^2 to 10^3 kJ mol^{-1}, which span the near IR, through the visible to the UV. A typical UV absorption spectrum contains two principle features. Above a certain energy or frequency known as the absorption edge, intense absorption occurs. To access frequencies above the absorption edge, reflectance techniques must be used. Charge transfer spectra, promotion of an electron from a localized orbital on one atom to a higher energy localized orbital on an adjacent atom, or promotion of an electron from a localized orbital on one atom to a delocalized energy band, the conduction band, can lead to an absorption edge. In electronically insulated ionic solids, the absorption edge may occur in the UV, but in photoconducting and semiconducting materials it may occur in the visible or near IR. Another feature is the

appearance of broad absorption peaks or bands at frequencies below that of the absorption cut-off. These are generally associated with promotion of an electron from a localized orbital on one atom to a higher energy localized orbital on the same atom. The associated absorption band is sometimes known as an exciton band. These can be d-d or f-f transitions in transition metal compounds. [20]

For UV-Vis spectroscopy, the following equations can be used to calculate important parameters such as band gap.

For direct band gap semiconductors:

$$\alpha(\hbar\omega) \propto \frac{\sqrt{\hbar\omega - E_{gap}}}{\hbar\omega} \tag{11}$$

where α is the absorption coefficient, hω is the energy of incident photons, and Eg is the electronic band gap of the semiconductor. Eg is the intercept of the straight line obtained by plotting $(\alpha\, h\omega)^2$ vs. hω.

For indirect band gap semiconductors:

$$\alpha(\hbar\omega) \propto \frac{(\hbar\omega - E_{gap})^2}{\hbar\omega} \tag{12}$$

Eg is the intercept of the straight line obtained by plotting the square root of (α hω) vs. hω.

The UV-Vis spectrometer used in these experiments was Perkin Elmer Lambda 950 UV/Visible/NIR Spectrophotometer.

4. Raman Spectroscopy

Raman spectroscopy is a spectroscopic technique used in condensed matter physics and chemistry to study vibrational, rotational, and other low-frequency modes in a system and used to diagnose the internal structure of molecules and crystals. When light interacts with a material, it can either be absorbed, scattered, or could pass through the material. If the photon interacts with the electron cloud of the material, it will be scattered. If the electron cloud distortion is the only interaction with the photon, then the frequency change of the photon will be very small, as the electrons in the cloud are relatively lighter. This is known as elastic scattering, or Rayleigh scattering. Rayleigh scattering is the dominant process. However, if the photon passes through the electron cloud and interacts with the nucleus, then energy is transferred from the photon to the molecule, or form the molecule to the photon. This is inelastic scattering, and is known as Raman scattering. The signal from Raman scattering is significantly weaker than Rayleigh scattering, as only one photon in every 10^6 to 10^8 will exhibit Raman scattering[21].

There are two mechanisms by which Raman scattering can occur. If the photon transmits energy to the molecule and excites it from the *m* vibrational ground state to and excited *n* state, then the scattering is known as Stokes scattering. However, if the molecule is already in an excited vibrational state, due to thermal energy or some other excitation, then the molecule will relax to the *m* state and transmit that energy to the

scattered photon. This is known as anti-Stokes scattering. Anti-Stokes scattering is significantly weaker than Stokes scattering and will become weaker as the excitations are conducted at lower temperatures. Typically, in Raman spectroscopy, only the Stokes scattering is taken into account [21]. A comparison of the excitations involved during Rayleigh, Stokes, and anti-Stokes scattering can be seen in Figure 10.

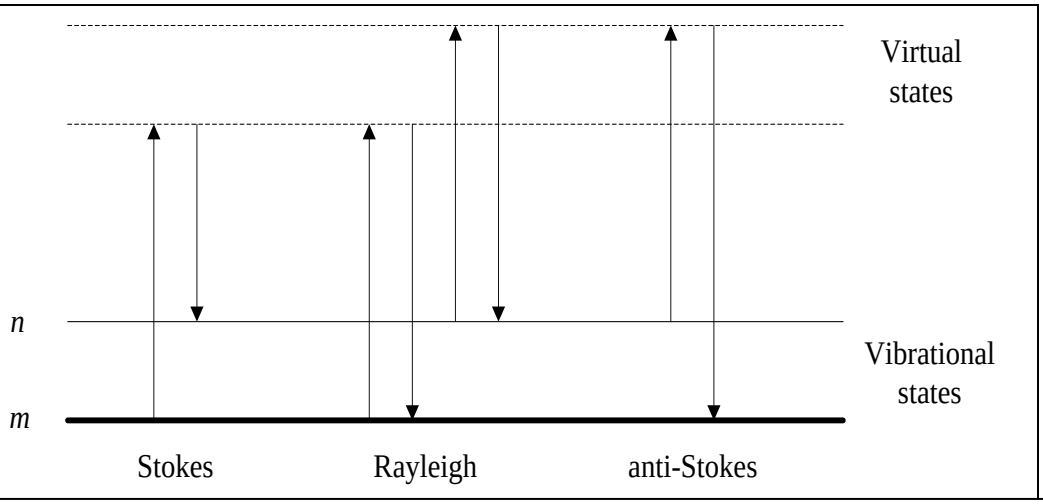

Figure 10: A diagram showing the change in the energy states of a molecule during interaction with a photon. Stokes and anti-Stokes scattering constitute Raman scattering. [18]

In a typical Raman scattering experiment, a monochromatic laser source is used. This laser could be Visible wavelengths, UV or NIR. Raman scattered light is frequency-shifted with respect to the excitation frequency, but the magnitude of the shift is independent of the excitation frequency. This "Raman shift" is therefore an intrinsic property of the sample. Because Raman scattered light changes in frequency, the rule of conservation of energy dictates that some energy is deposited in the sample. A definite Raman shift corresponds to excitation energy of the sample (such as the energy of a free vibration of a molecule). In general, only some excitations of a given sample are "Raman active," that is, only some may take part in the Raman scattering process. Therefore, the frequency spectrum of the Raman scattered light maps out part of the excitation

spectrum. Other spectroscopic techniques, such as IR absorption, are used to map out the non-Raman active excitations.

A Raman spectrum is a plot of the intensity of Raman scattered radiation as a function of its frequency difference from the incident radiation (usually in units of wave numbers, cm^{-1}). This difference is called the Raman shift. The instrument used to measure the Raman spectra in these experiments is the Renishaw inVia Raman Microscope. The red laser used for the Raman excitation is a Renishaw RL633 Lazer.

The reactors used in these experiments operate on very simplistic concepts, such as a heated metal wire and a hot plate. These reactors can be easily be scaled up for industrial purposes. The simplistic reactor design and consistency in the results allow for this technology to be easily implemented in a variety of applications.

IV. RESULTS AND DISCUSSION

This chapter presents the reaction parameters for the synthesis of Molybdenum oxide nanowire arrays, then the conditions for conversion into Molybdenum sulfide. Then, the results of the various characterization techniques are presented.

A. Synthesis MoO_3 Nanowire Arrays

The first step in attempting to convert Molybdenum oxide nanowires to Molybdenum sulfide is to actually produce the oxide nanowire array. Previously, the HFCVD reactor reliably produced WO_3 nanowire arrays, so theoretically, the synthesis of MoO_3 NW arrays was possible, but the operating parameters had to be investigated.

During the first set of experiments, pure oxygen was flown into the system at a constant flow rate, while the filament temperature was adjusted to find the optimal conditions. The oxygen flow rate was set at 15 sccm, which was based on experimental conditions for WO_3 synthesis. Initially, 35 Volts were applied to the filament, yielding a temperature of 1200°C. The system was operated for 10 minutes, again based upon WO_3 synthesis techniques. The high temperature yielded a "chip" morphology, which can be seen in Figure 11.

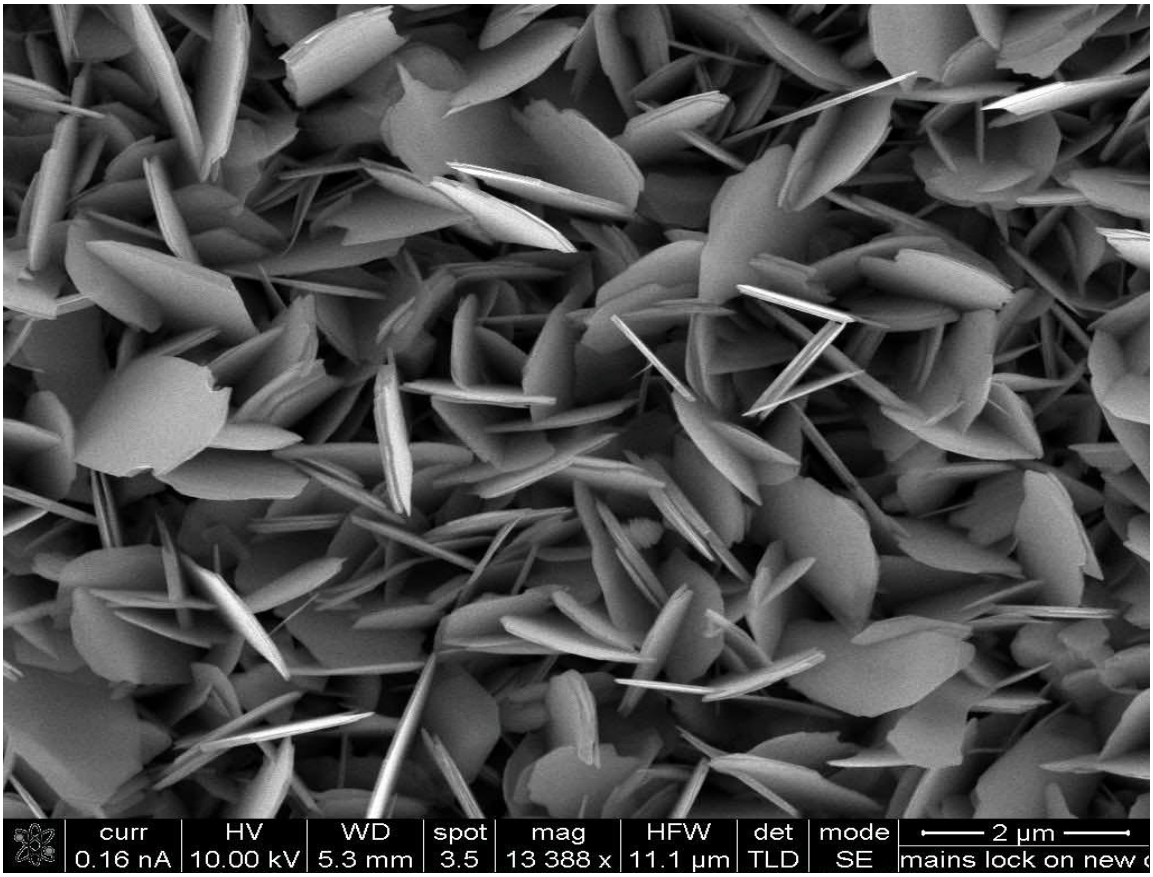

Figure 11. MoO_3 nano-particles exhibiting a "chip" morphology. This morphology results from higher filament temperatures.

The samples were opaque and white with a light blue tint. As the temperature was decreased, nanowires could be seen growing off the edge of the "chips". If the temperature was too low, then relatively no deposition would occur.

The oxygen flow rate was then lowered to 10 sccm, which yielded consistent nanowire arrays at a filament temperature of approximately 775°C. The operating pressure ranged from .7 to .9 Torr. 20 – 25 Volts were applied to the filament, which yielded 200 W. The nanowire arrays can be seen in Figure 12.

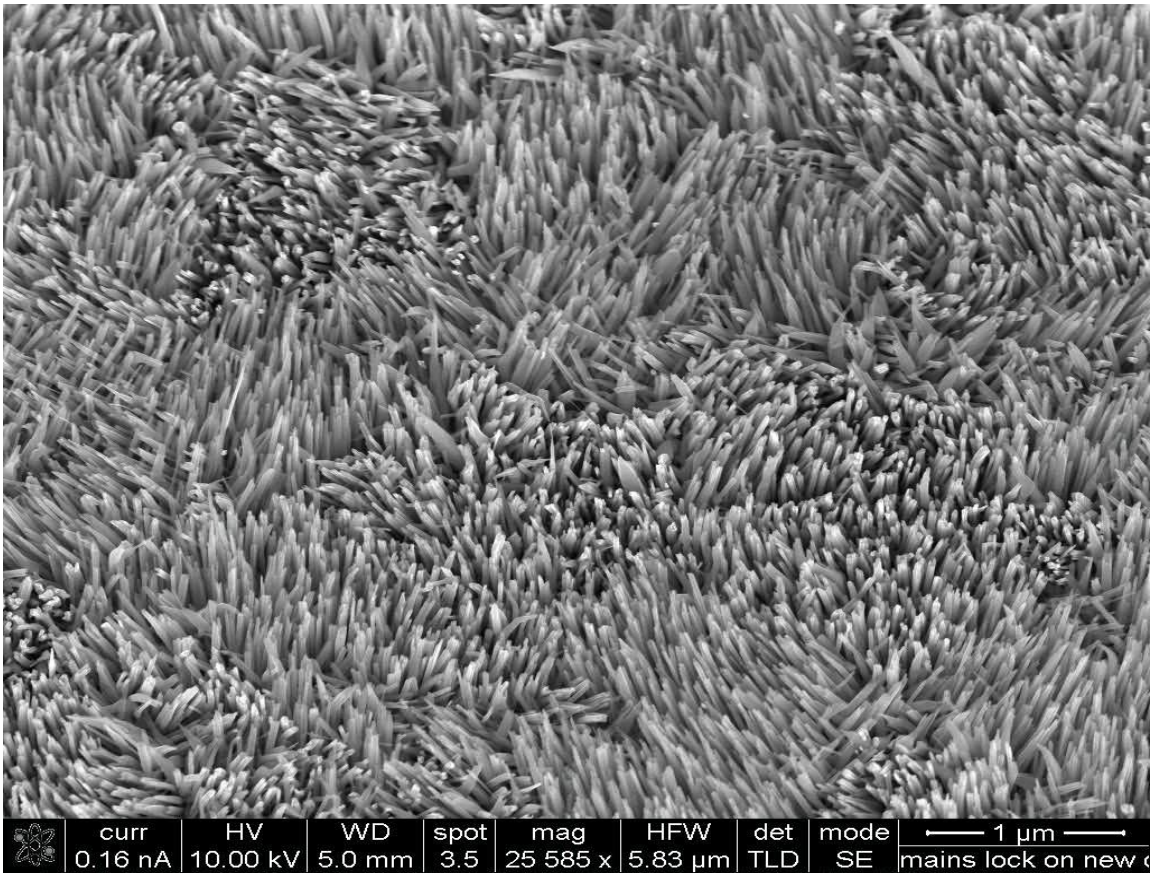

Figure 12. SEM image of MoO_3 nanowire array on quartz.

Once MoO_3 was successfully deposited onto FTO glass, it was then attempted to deposit the nanowires onto quartz substrates. The quartz substrates were not as thick at the FTO substrates, so, theoretically, the surface would heat up more quickly. Slightly less voltage was applied to the filament and nanowire arrays were successfully grown on the quartz substrates. The difference in thickness made little difference in the synthesis conditions. It was found that longer, more consistent nanowire growth was obtained by increasing the reaction time from 10 minutes to 30 minutes. It appears, based on the observations, that the majority of MoO_3 NW array deposition occurs while the reactor is cooling.

B. Sulfurization of MoO_3 NW Arrays

1. Thermodynamic Analysis

The Gibb's free energy of the possible sulfurization reactions was calculated using JANAF Thermochemical Data Tables. [22] The first reaction analyzed was the conversion of MoO_3 to MoS_2.

$$MoO_3 + 2\ H_2S \rightarrow MoS_2 + 2\ H_2O + ½\ O_2$$

The Gibb's energy of this reaction can be seen in Figure 13. At temperatures reached in the reactor, this reaction is very endergonic, which indicates this reaction is not spontaneous.

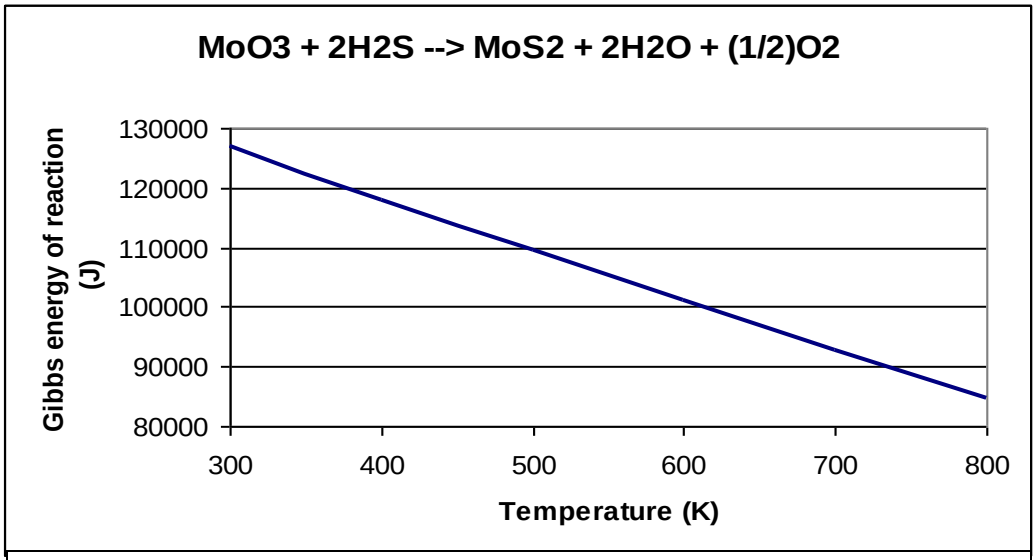

Figure 13. Plot of Gibb's Free Energy versus Temperature. This reaction is not spontaneous.

The next reaction investigated involves the conversion of a reduced for of molybdenum oxide, MoO_2.

$$MoO_2 + 2H_2S \rightarrow MoS_2 + 2H_2O$$

The Gibb's energy of this reaction was also calculated. The change in Gibb's energy with temperature can be seen in Figure 14. This reaction is very spontaneous at the reactor conditions.

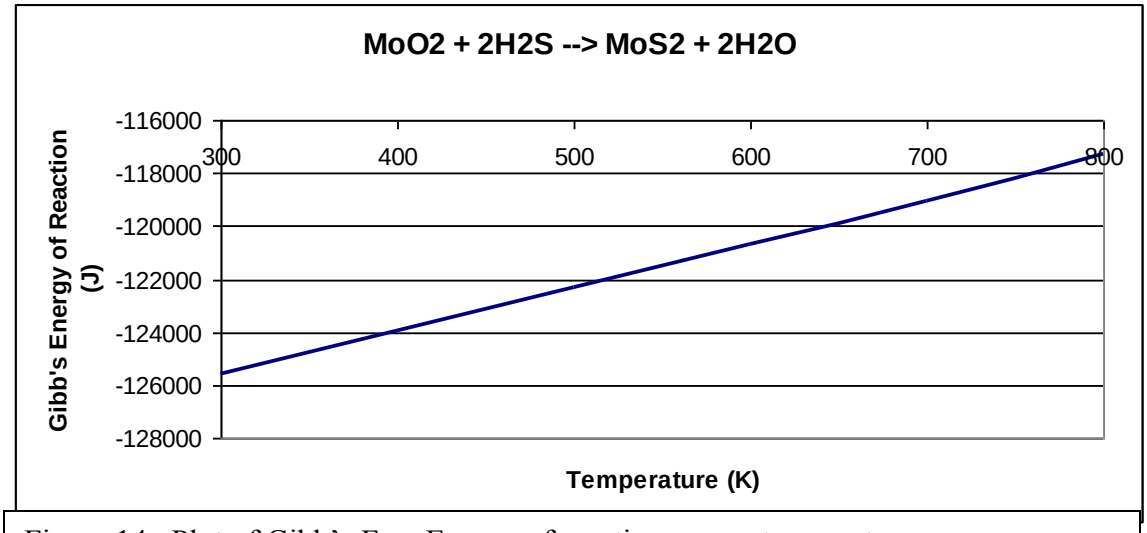

Figure 14. Plot of Gibb's Free Energy of reaction versus temperature.

Based on the thermodynamic analysis, it is very likely that the reduced form of the oxide, MoO_2, is the reactive form and more easily forms molybdenum sulfide.

2. Sulfide Reaction

The oxide sample was placed into the reactor and 1000 ppm H_2S with Helium as a carrier gas was flown into the system. Initially, the reactor was set at temperature around 800°C and allowed to react for 1 hour. Upon examining the sample after the reaction, it was observed that all of the MoO_3 had vaporized in the chamber, leaving essentially a

clean piece of quartz. MoO_3 was found to sublime at approximately 700°C [23], so the reaction conditions must be kept significantly below this temperature. Also, 1000 ppm of reactant in an inert gas is not a high enough concentration to overcome the diffusion limits of the oxide to sulfide reaction, so the switch was made to pure H_2S. Since the use of pure H_2S significantly increases the safety issues of the reaction, the cylinder and MFC were kept in a fume hood and fed to the reactor.

A 25 sccm of H_2S was fed to the system. A substrate temperature of 390°C, measured by thermocouple, was obtained using an applied voltage of 17.5 V to the heater. The pressure of the system stayed relatively constant at 0.06 Torr and the reaction ran for 1 hour. The sample changed color from its original transparent light blue, to an opaque black. XRD analysis shows that the sample had some peaks corresponding to MoS_2, and others from MoO_3, which indicates that the reaction did not come to completion. It was decided to increase the reaction time, since it seemed to be limited by the diffusion of H_2S into the oxide nanowires. Some other researchers [24] have used H_2 in conjunction with lower hydrogen disulfide flow rates to successfully synthesize MoS_2. The typical reaction for the synthesis involves the reduced form of Molybdenum oxide, MoO_2:

$$MoO_2 + 2H_2S \rightarrow MoS_2 + 2H_2O$$

The presence of hydrogen in the reaction could act as a reducing agent to facilitate the sulfurization reaction. So, H_2 was fed to the system in a 2:1 ratio to H_2S. The temperature was lowered to 340°C and allowed to react for 3 hours. XRD analysis

showed that the sample was reduced to MoO_2 with essentially no sulfide formation. Since better results had been achieved with pure H_2S, it was decided to abandon the Hydrogen approach.

A 25 sccm of H_2S was flown over the substrate with a reaction pressure of 0.5 Torr. The substrates were maintained at a reaction temperature between 250 and 300°C by applying 15 Volts to the hot plate. The reaction was allowed to proceed for 3 hours, then the reactor was cooled under vacuum. The sample was again opaque and black. But under XRD analysis, it was found that MoS_2 was in the sample, along with traces of MoO_2. The presence of the reduced oxide shows that the reaction did not come to completion, as the diffusion limits for the reaction are very high. However, the properties were noticeably changed from the oxide.

An SEM image of the MoS_2 nanowire arrays can be seen in Figure 15. These synthesized wires were on the average 0.5 microns long, with diameters ranging from 10 - 20 nm.

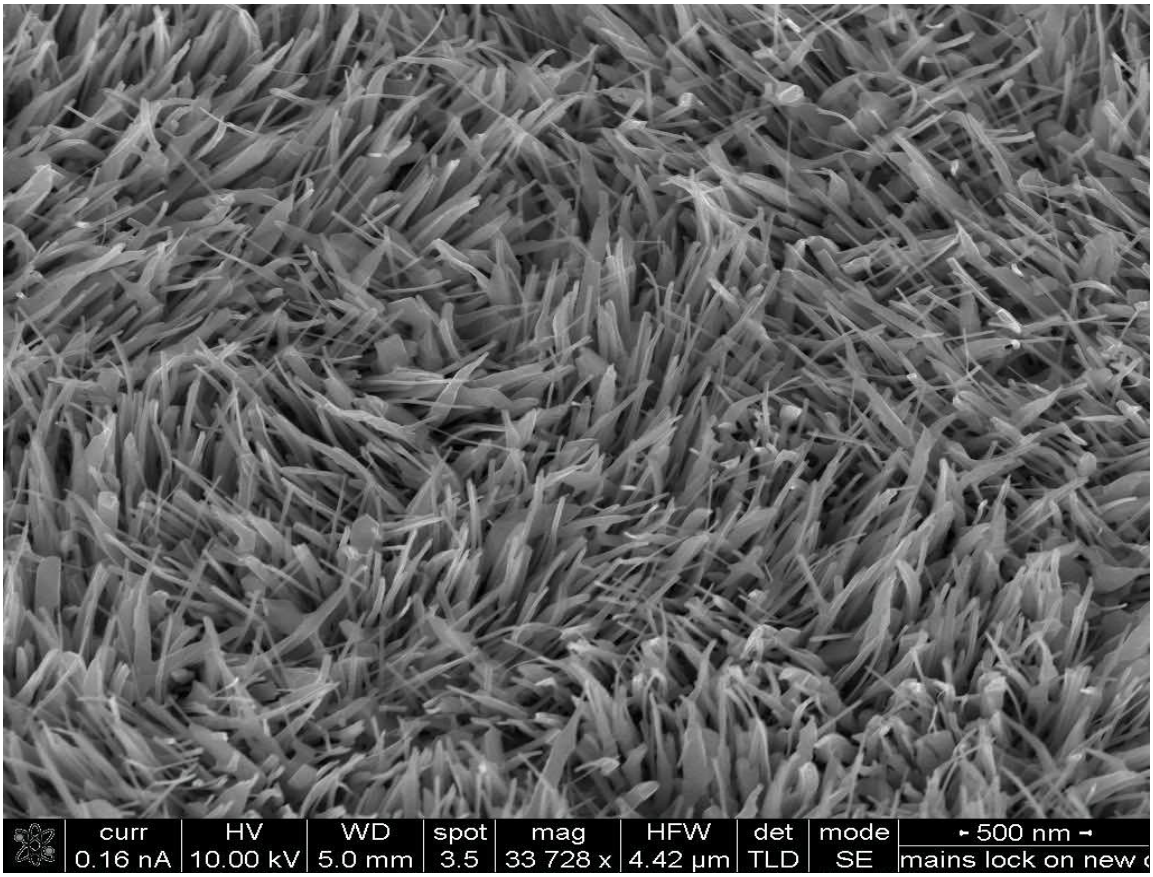

Figure 15. SEM image of MoS_2 nanowire array on quartz.

C. Characterization

The chemical composition of the MoO_3 nanowire array was determined by X-Ray diffraction. The XRD spectrum with the reference spectrum of MoO_3 can be seen in Figure 16. The XRD spectra of the MoS_2 nanowire array can be seen in Figure 17.

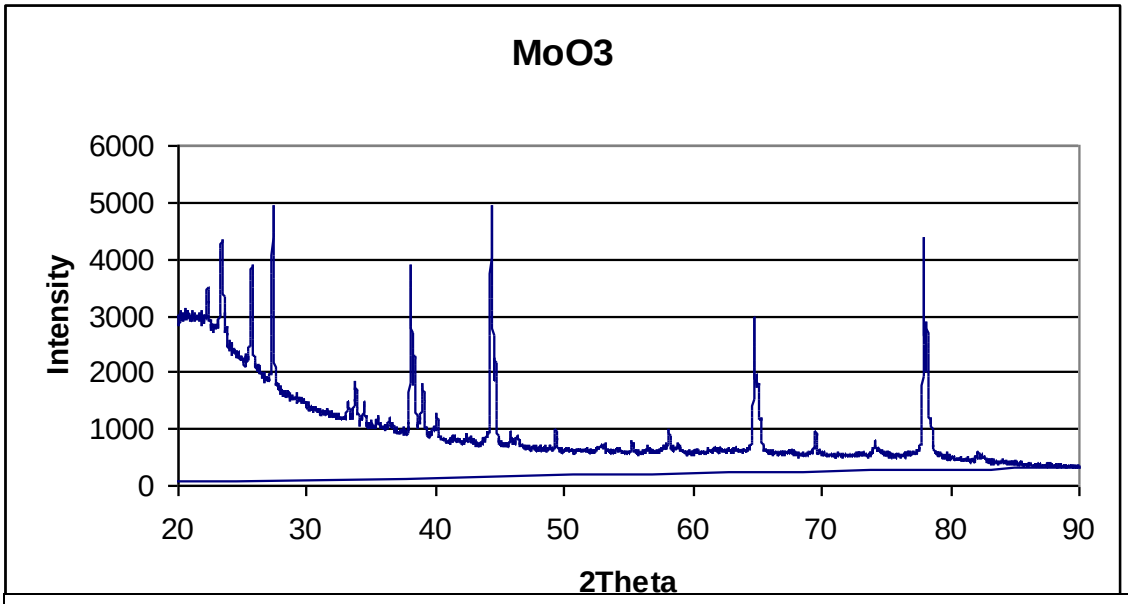

Figure 16. XRD spectrum of MoO_3 nanowires on quartz substrate.

The peaks at 77° and 43° are from the quartz substrate. This spectrum shows very clearly that the sample is entirely MoO_3. Figure 17 shows the spectrum for the sample once it had undergone the sulfurization reaction.

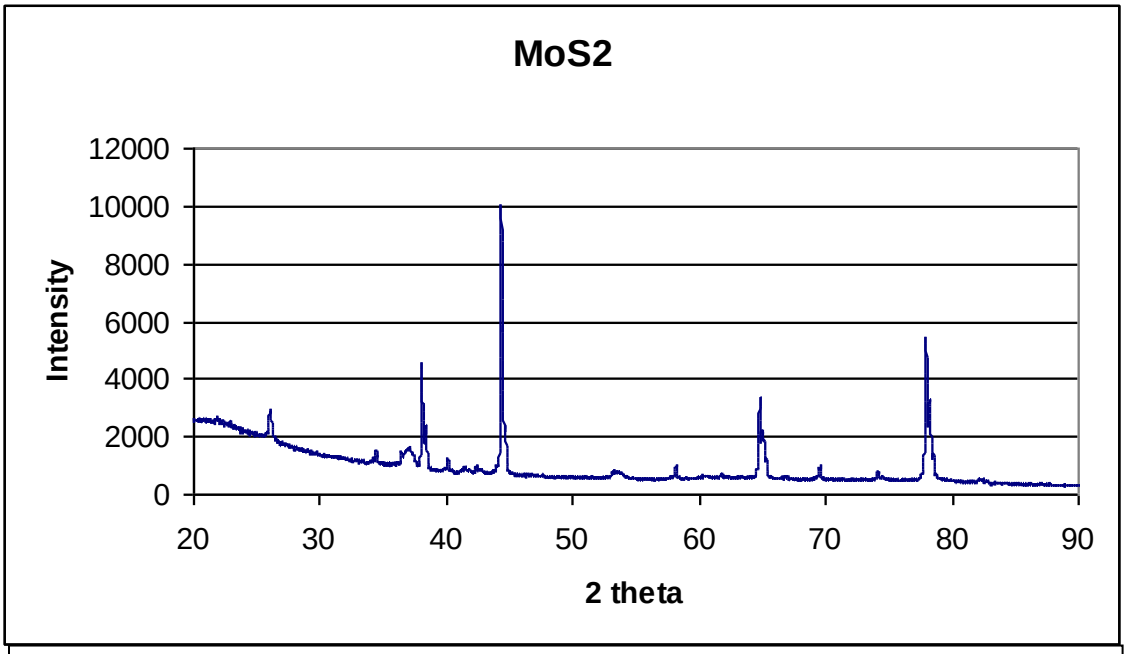

Figure 17. XRD spectrum for MoS_2

It very clearly shows that MoO_3 is no longer present in the sample. Some peaks of MoS_2 can be seen, but also the reduced form of Molybdenum oxide, MoO_2 can also be seen. This shows that the diffusion limit of the sulfide gas into the oxide nanowires is very high. The reaction did not go to completion, but the reaction proceeded far enough to achieve noticeable changes in properties

The band-gap the MoO_3 nanowire array was determined by UV-Vis spectroscopy. A plot of absorption versus wavelength can be seen in Figure 18.

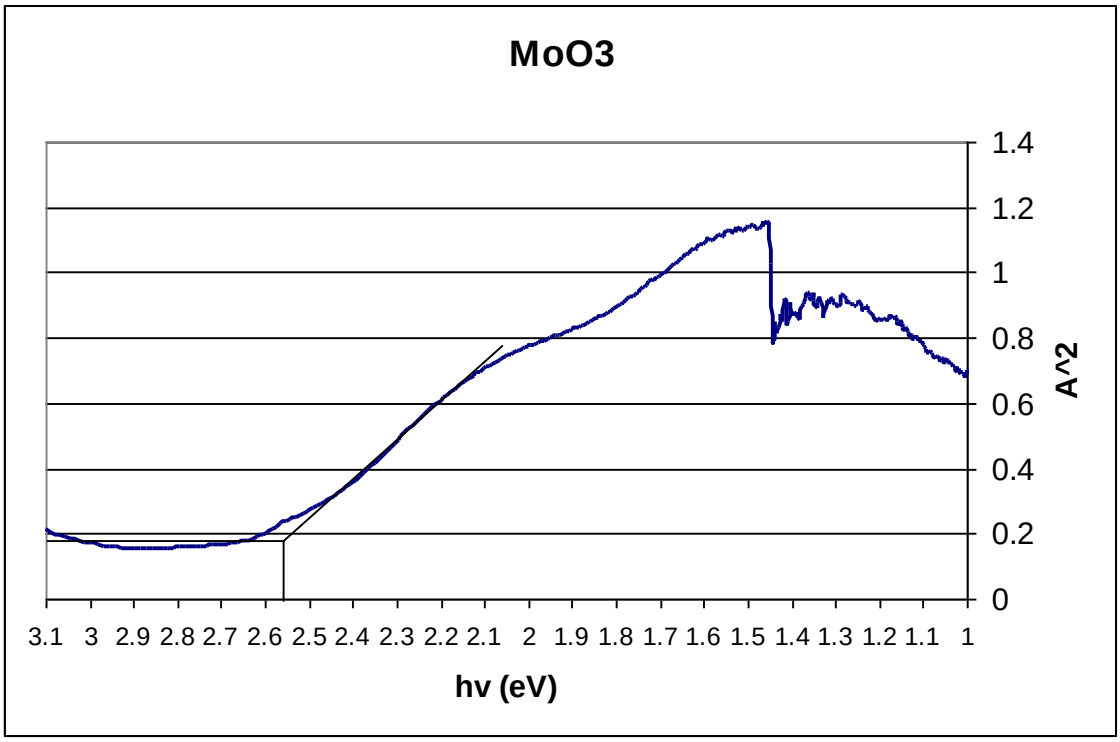

Figure 18. UV-Vis spectrum of MoO_3 nanowire array on quartz. The spike at 858 nm occurs because of the switching of lamps in the instrument.

The absorption edge can be clearly seen in the visible range. Drawing a straight line following the absorption edge yields a band gap energy of 2.55 eV. Based on the UV-Vis data, it can be shown that MoO_3 nanowires are a direct band gap material.

The results of the UV-Vis analysis for the MoS_2 nanowires can be seen in Figure 19. It can be shown that MoS_2 has an direct band gap of 1.45 eV. This differs slightly from the band gap value found in literature for bulk MoS_2 of 1.2 eV. [12]

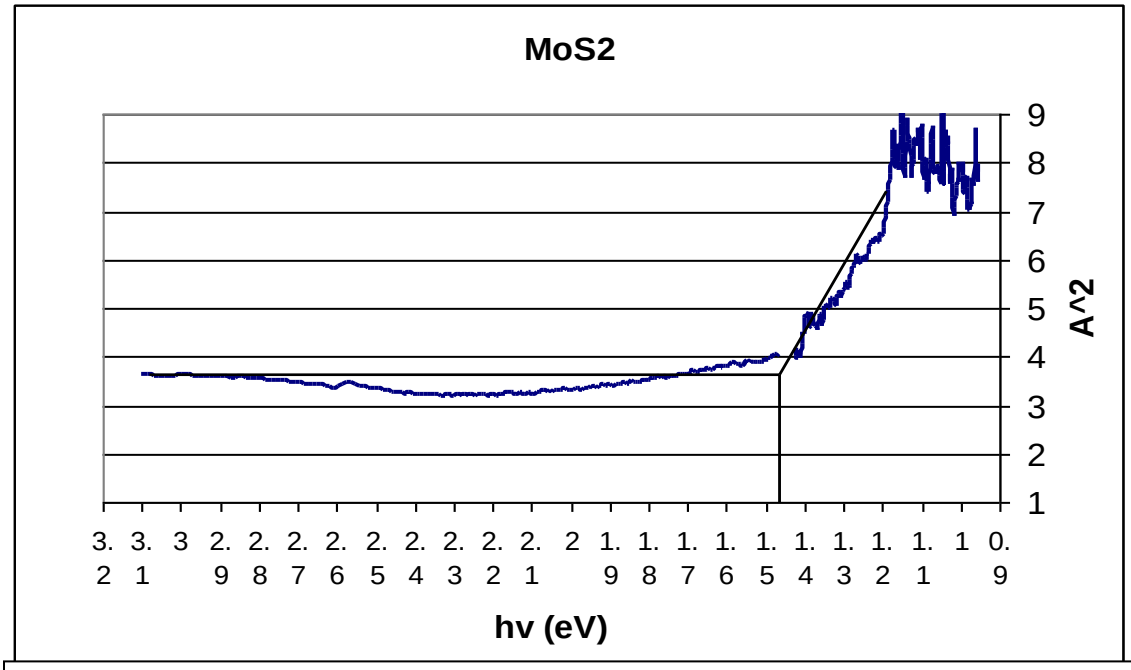

Figure 19. UV-Vis spectrum of MoS_2 on quartz.

Visual Photoluminescence was conducted on the molybdenum sulfide sample. The analysis was conducted at -100°C for a more accurate band gap determination. The cold PL spectrum can be seen in Figure 20. Based on this data, a band gap of approximately 2.1 eV was found for MoS_2. Since the analysis was performed at significantly lower temperatures, there will be a difference between the UV-Vis determined band gap and PL.

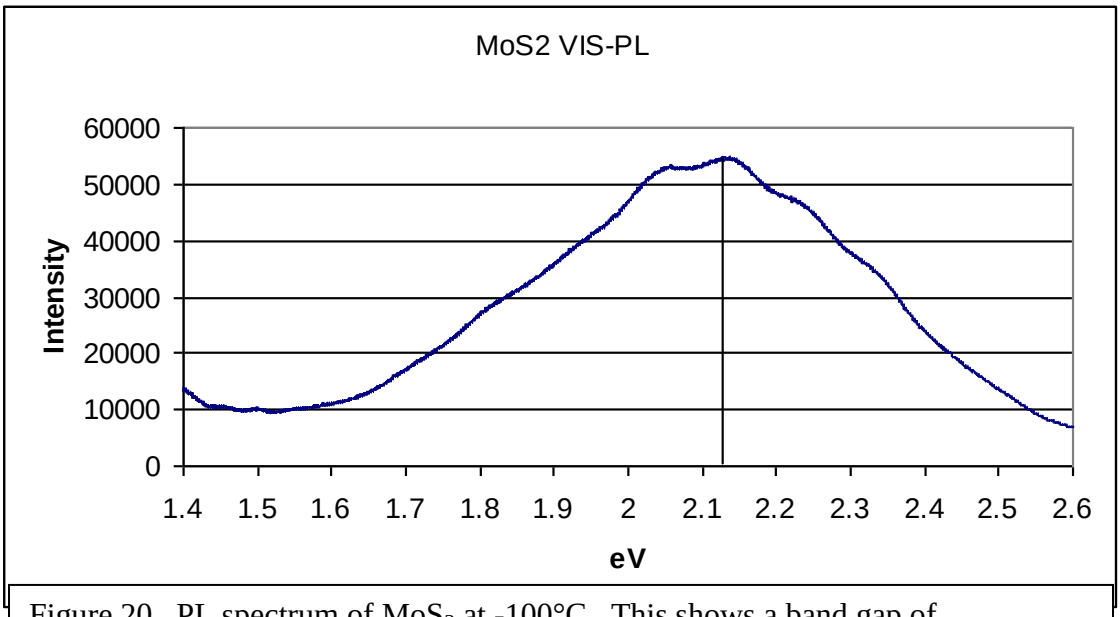

Figure 20. PL spectrum of MoS_2 at -100°C. This shows a band gap of approximately 2.1 eV.

Raman spectroscopy was performed on both the MoO_3 and the MoS_2 samples. It was conducted at room temperature and recorded visible Raman, meaning that it was excited with a laser with a wavelength of 632 nm. Since small variations in the Mo-O bonding and Mo-S bonding can cause large variations in Raman peaks, the Raman spectra were used merely as a comparative tool to show the change from oxide to sulfide. The Raman spectra for MoO_3 and MoS_2 can be seen in Figure 21 and 22, respectively.

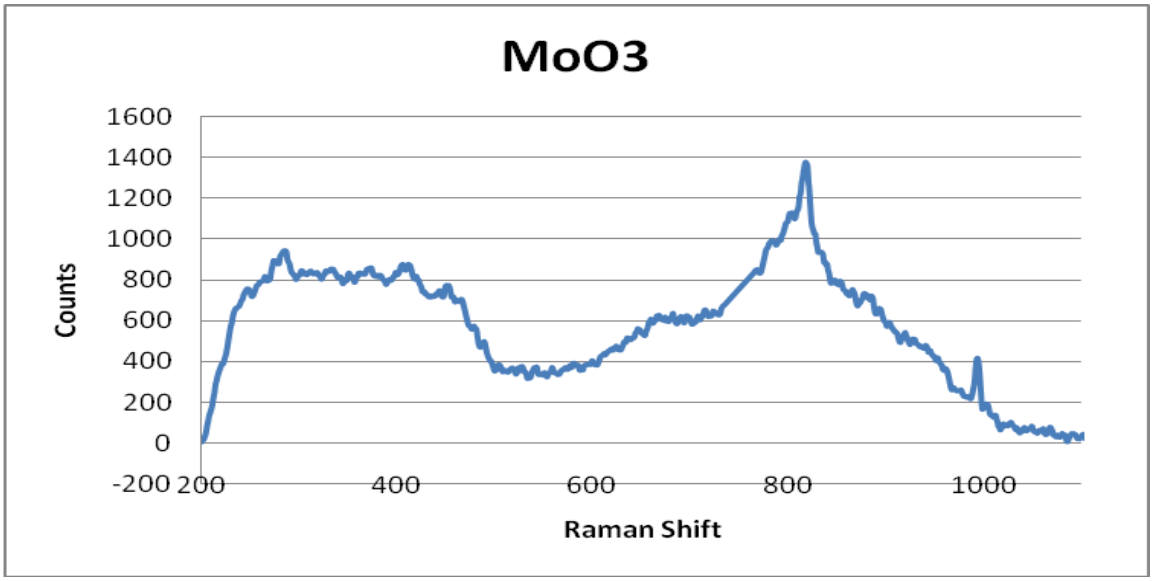

Figure 21. Raman spectra of MoO_3 nanowires on quartz, excited with 632 nm Red laser.

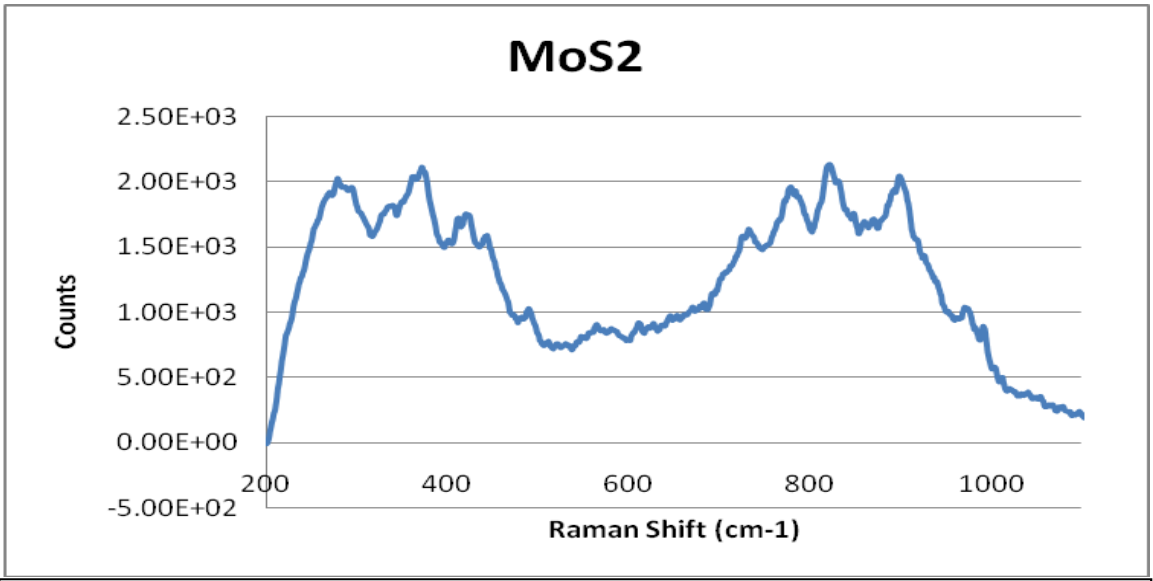

Figure 22. Raman spectra of MoS_2 nanowires on quartz, excited with 632 nm Red laser.

The prominent peak in at 825 cm^{-1} the MoO_3 spectrum also appears in the MoS_2, which implies that the reaction did not go to completion. But, the MoS_2 also has peaks at 905 cm^{-1}, 790 cm^{-1}, and 740 cm^{-1} which indicates that clearly a large part of the nanowires are

MoS_2. The peaks ranging from 250 to 500 cm^{-1} have a higher intensity in the MoS_2 spectra than the MoO_3 spectra, which indicates a compositional change.

In addition to Raman and XRD, Electron Diffraction Spectroscopy (EDS) is a very popluar and quick method to determine the elemental composition of a sample. It operates in conjcution with an SEM by collecting high energy electrons emitted from the sample. Each element has a very distinctive electron energy, so the elemental compositon and relative proportions of those elements in a smaple can be determined easily. EDS is an effective method to determnine the presence of MoO_3, however it is unable to effectively detect MoS_2. The reason is that the core electron energies of Molybdenum and Sulfur are so close that the instrument could not differentiate between the two. Molybdenum has a K orbital energy of 17.481 eV and the energy of its L orbital is 2.293 eV. The K orbital energy for Sulfur is 2.307 eV. The L orbital energy of Mo, which is the most prominent peak, and the K orbitale energy of S are very similar. These energies are too similar for the instrument to differentiate, therefore EDS was not used in these experiments.

Based on these results, MoO_3 nanowire arrays were successfully formed and can be easily reproduced. It seems that the diffusion limits during the sulfurization reaction are very great and it is difficult to completely convert molybdeum oxide to sulfide. However, enough of the sample was converted to give noticeable changes in properties, especially a significantly lower band gap energy.

V. CONCLUSIONS

In this thesis, the synthesis of Molybdenum oxide nanowire arrays on both FTO glass and quartz was shown. Then, these oxide nanowires were reacted with Hydrogen disulfide to produce Molybdenum sulfide nanowires. This reaction did not go to completion, but proceeded far enough to cause a noticeable change in properties. The following conclusions can be drawn from these results:'

- The optimal conditions for reliable growth of Molybdenum oxide nanowires are at a low pressure ranging from 0.7 to 0.9 Torr, with a pure oxygen flow rate of 10 sccm. 200 W of power is applied to the Molybdenum filament, yielding a filament temperature of ~775°C.
- Molybdenum sulfide was formed by passing 25 sccm of H_2S at a pressure of approximately 0.5 Torr. 15 Volts were applied to the hot plate, which yielded a reaction temperature of 250 to 300°C. The reaction was run for 3 hours.
- The diffusion limit of the sulfide gas through the oxide nanowire is very high. It can be shown through XRD that the reduced form of the oxide, MoO_2, is present along with Molybdenum sulfide. The reaction proceeded far enough to cause noticeable changes in the material properties, significantly lowering the band gap energy.

VI. RECOMMENDATIONS

In order to make improvements on this work, recommendations are:

- Incorporate a thermocouple into the HFCVD reactor set-up. This would allow for a reliable reading of the substrate temperature and would increase the reproducibility of the results. The only issue is that the samples are slid in and out of the reactor after each experiment, so the thermocouple would have to be removed and replaced each time, which could prove problematic.
- More experiments need to be done involving a Hydrogen stream in the sulfurization reaction. The goal is to fully convert Molybdenum oxide to molybdenum sulfide, and the use of a reducing agent, such as H_2, should be pursued.
- Work has already began researching MoO_3 nanowires as an anode in Lithium battery technology. MoS_2 nanowires should also be investigated as a cathode material in batteries. These materials hold great promise for improvement to this technology.

WORKS CITED

[1] Y.S. Jung, S. Lee, D. Ahn, A.C. Dillon, S.H. Lee, J. Power Sources 188 (2009) 286-291.

[2] C. Julien, S.I. Saikh, G.A. Nazri, Mater. Sci. Eng. B-Solid State Mater. Adv. Technol. 15 (1992) 73-77.

[3] J. Chen, N. Kuriyama, H. Yuan, H.T. Takeshita, T. Sakai, J. Am. Chem. Soc. 123 (2001) 11813-11814.

[4] J. Chen, S.L. Li, Z.L. Tao, J. Alloy. Compd. 356 (2003) 413-417.

[5] R.S.a.W.C.E. Wagner, Applied Physics Letters 4 (1964) 89-90.

[6] J.M. Prausnitz, R. N. Lichtenthaler, and E. G. Azevedo Molecular Thermodynamics of Fluid-Phase Equilibria, 3 ed., Prentice Hall PTR, New Jersey, 1999.

[7] H. Chandrasekaran, Rationalizing Nucleation and Growth in the Vapor-Liquid-Solid (VLS) Methods, Chemical Engineering, University of Louisville, Louisville, 2006.

[8] F.C. Frank, Discussions of the Faraday Society 5 (1949) 48-54.

[9] R. Thurman, Bulk Synthesis of Metal Oxide Nanowires, Chemical Engineering, University of Louisville, Louisville, 2006, p. 82.

[10] J.A. Venables, Thermodynamics versus Kinetics, Arizona State University, 2003.

[11] S. Vaddiraju, H. Chandrasekaran, M.K. Sunkara, J. Am. Chem. Soc. 125 (2003) 10792-10793.

[12] G. Nagaraju, C.N. Tharamani, G.T. Chandrappa, J. Livage, Nanoscale Research Letters 2 (2007) 461-468.

[13] L.F. Flores-Ortiz, M.A. Cortes-Jacome, C. Angeles-Chavez, J.A. Toledo-Antonio, Solar Energy Materials and Solar Cells 90 (2006) 813-824.

[14] Y.F. Shi, Y. Wan, R.L. Liu, B. Tu, D.Y. Zhao, J. Am. Chem. Soc. 129 (2007) 9522-9531.

[15] H.A. Therese, N. Zink, U. Kolb, W. Tremel, Solid State Sciences 8 (2006) 1133-1137.

[16] J. Thangala, S. Vaddiraju, S. Malhotra, V. Chakrapani, M.K. Sunkara, Thin Solid Films 517 (2009) 3600-3605.

[17] G. Goldstein, D. Newbury, P. Echlen, D. Joy, C. Fiori, E. Lifshin, Scanning electron microscopy and x-ray microanalysis, Plenum Press, New York, 1981.

[18] I. Watt, Principles and Practices of Electron Microscopy, 2nd ed., University Press, Cambridge, 1997.

[19] B.D. Cullity, and S.R. Stock, Elements of X-Ray Diffraction, 3rd ed., Prentice Hall, Upper Saddle River, NJ, 2001.

[20] A.R. West, Basic Solid State Chemistry, 2nd ed., John Wiley & Sons, New York, 1999.

[21] E. Smith, Geoffrey Dent, Modern Raman Spectroscopy: A Practical Approach, John Wiley & Sons, New York, 2005.

[22] M.W. Chase, NIST - JANAF thermochemical tables, 4th ed., American Institute of Physics for the National Institute of Standards and Technology, Woodbury, NY, 1998.

[23] C.H. Wang, C.N. Lee, H.S. Weng, Ind. Eng. Chem. Res. 37 (1998) 1774-1780.

[24] A. Rothschild, J. Sloan, R. Tenne, J. Am. Chem. Soc. 122 (2000) 5169-5179.

VITA

Dustin Ray Cummins was born in Ft. Riley, Kansas on June 11, 1987. His father, Monty Cummins, died when he was seven years old, so from then on he was raised by his mother, Faith Cummins. He currently lives in Erlanger, KY, which is suburb of Cincinnati OH.

Dustin attended high school at the Covington Latin School and graduated in 2004. He achieved his Bachelor's degree in Chemical Engineering from the University of Louisville in 2008. He will graduate with his Masters of Engineering degree in 2009.

Dustin did 3 engineering co-ops at The Dallas Group of America, Inc., which produce synthetic magnesium silicates for use in purifying frying oils and biodiesel.

Upon completion of his Master’s degree, Dustin will continue his education at the University of Louisville to obtain his PhD in Chemical Engineering.